Positron annihilation analysis of micropores and growth mechanism of oblique angle evaporated TiO_2 and SiO_2 thin films and multilayers

Aurelio García-Valenzuela,[1] Maik Butterling,[3] Maciej Oskar Liedke,[3*] Eric Hirschmann,[3] Thu Trang Trinh,[3] Ahmed G. Attallah,[3] Andreas Wagner,[3] Rafael Alvarez,[1,2] Jorge Gil-Rostra,[1] Victor Rico,[1] Alberto Palmero,[1] Agustín R. González-Elipe[1*]

1. *Nanotechnology on Surfaces Laboratory. Instituto de Ciencia de Materiales de Sevilla (CSIC-Univ. Sevilla). Avda. Américo Vespcuio 49. 41092 Sevilla. Spain.*
2. *Departamento de Física Aplicada I. Escuela Politécnica Superior, Universidad de Sevilla. c/ Virgen de África 7, 41011, Seville, Spain*
3. *Institute of Radiation Physics, Helmholtz-Zentrum Dresden-Rossendorf, Bautzner Landstrasse 400, 01328 Dresden, Germany*

Corresponding authors: *arge@icmse.csic.es;
* m.liedke@hzdr.de

Keywords: positron annihilation, micropores, OAD thin films, TiO2, SiO2, growing mechanism

Abstract

The micro- and nano-porosity embedded into the tilted and separated nanocolumns characteristic of the microstructure of evaporated thin films at oblique angles has been critically assessed by various variants of the positron annihilation spectroscopy (PAS). This technique represents a powerful tool for the analysis of porosity, defects and internal interfaces of materials, and has been applied to different as-deposited SiO_2, TiO_2 thin films and SiO_2/TiO_2 multilayers prepared by electron beam evaporation at 70º and 85º zenithal angles. It is shown that, under same deposition conditions, the concentration of internal micro and nano-pores in SiO_2 is higher than in TiO_2 nanocolumns, while the TiO_2/SiO_2 multilayers represent an intermediate situation. These features have been explained by considering the influence of the chemical composition on the growth mechanism and, ultimately, on the structure of the films.

1.-Introduction

During the last years, Oblique Angle Deposition (OAD) of thin films has emerged as a suitable methodology to control their nano and microstructure [1,2]. When grown at low temperatures by evaporation, these are formed by tilted and well-separated nanocolumns with typical diameters in the order of few tens nm and a high porosity, containing both large pores separating the columns (i.e. mesopores connected with air) and small occluded pores, likely distributed inside the nanocolumns [3,4]. This particular microstructure has been widely utilized for a large variety of applications in optics, electrochemistry, catalysis, solar, cells, batteries and several other fields and topics where an open and nanostructured morphology is a requirement [1, 5-10]. Despite the numerous experimental evidences on the high porosity of these thin films, including some specific studies on pore characteristics and pore size distribution [11, 12], its description is by no means complete. For example, it is widely accepted that small occluded nanopores (i.e. micropores according to the IUPAC terminology [13]) are scattered inside the nanocolumns [12] However, to our knowledge, clear experimental evidences sustaining this assertion or relevant data on their size and other features are still missing in the literature.

Much effort regarding the OAD deposition of thin films in the last years have been put to unveil the mechanism by which gaseous species are deposited onto a substrate and how this mechanism controls the formation of the tilted nanocolumnar structures. In particular, this research has focused on the intrinsic connection between the deposition conditions, i.e. angle of incidence of deposition species onto the substrate and the chemical composition of the growing film, and the tilt angle of the emerging columnar structures [14,15]. Within this context, the so-called tangent [16] and cosine [17] rules were proposed as empirical relations linking the tilt angle of the nanocolumns and the deposition angle. Yet, these rules fail for large deposition angles and do not always explain the observed trend as a function of the chemical composition of the material. In a recent publication, we have proposed that the governing growth mechanism, namely the surface shadowing mechanism, is highly affected by short-range interactions between gaseous species and the film surface, responsible for bending the trajectory of the former and changing its landing position [18]. We dubbed this process *surface trapping mechanism* and expressed its efficiency in terms of a trapping factor or probability, s_t, dependent on the nature of the gaseous species and on the film chemical composition, e.g. $s_t = 0$ for metals, $s_t \sim 0.1$ for TiO_2 or $s_t = 1$ for other oxides such as SiO_2 thin films [18]. Besides successfully accounting for the tilt angle of nanocolumns of different materials, this mechanism also implies the existence of intrinsic differences in

porosity depending on the chemical composition of the films, including the possible internal porosity in the nanocolumns, a result that has not yet been verified in the literature.

The present work addresses this problem by using the positron annihilation spectroscopy (PAS) technique to analyze the actual porosity and pore size distribution in the interior of nanocolumns of TiO_2 ($s_t \sim 0.1$) and SiO_2 ($s_t = 1$) thin films and multilayers. This method is sensitive to lattice defects, grain interfaces and very small pores [19-22] and has been widely utilized for the characterization analysis of bulk [23-25] and layered materials [26, 27]. In relation with the present work PAS would be sensitive to micropores as those expected to exist in the nanocolumns of thin films. In other words, this technique will specifically describe the micropores existing within the nanocolumns and will disregard the large mesopores defining the intercolumnar voids. The obtained results have been discussed under the light of the main mechanisms governing the film growth, i.e. surface shadowing processes, and surface trapping mechanisms, [28, 29] and have provided a general methodology relating the mechanistic description of deposition and the empirical analysis of microporosity in thin films prepared by physical vapor deposition procedures.

2.-Experimental and methods

2.1.-Thin films and multilayers

TiO_2 and SiO_2 thin films of thicknesses ~600 nm were grown on a silicon wafer by electron beam-assisted evaporation from TiO and SiO_2 crucibles in $1x10^{-4}$ torr oxygen to ensure the complete oxidation of the deposited films. Films were grown at two different zenithal angles of evaporation: 70º and 85º. Distance between crucible and substrates was approximately 500 mm. Further details about the preparation of this kind of OAD thin films and about their basic characteristics can be found in previous publications [4, 30, 31]. These samples are designated as SiO2-α and TiO2-α, where α denotes the deposition angle. Moreover, TiO_2/SiO_2 multilayers consisting of five stacked layers of TiO_2 and SiO_2 single layers of approximately 110 nm thick (i.e., total thickness of 550 nm, equivalent to that of the studied single oxide films of SiO_2 and TiO_2) were prepared by the successive deposition of the two oxide materials at two zenithal angles, 70º and 85º. After the deposition of each monolayer, the substrate was azimuthally rotated 180º [32], a change well-known for rendering a *zig-zag* arrangement of the nanocolumns.

Two sets of equivalent SiO_2 and TiO_2 thin film samples were analyzed. A first set was prepared as already described and used for the PAS analysis without further modifications. A similar second set of nanostructured SiO_2 and TiO_2 thin film samples was covered by a thin and compact SiO_2 layer with a thickness ranging between 100 and 200 nm. This homogenous layer is intended to act as a *capping layer*, which was

intentionally grown to analyze its influence on the PAS analyses. SiO_2 *capping layers* were fabricated by plasma enhance chemical vapour deposition (PECVD) using dimetyldisiloxane (DMSO) as silicon precursor. The process was carried out in a vacuum chamber equipped with flow controlled systems of Ar, O_2 and DMSO, and a radio frequency (RF) polarizable and rotatable sample holder. The plasma source was an RF generator (Hunttinger PFG300FR) operated at 50W. The process gas consisted of a mixture of Ar (10 sccm), O_2 (17.5 sccm) and DMSO (4.5 sccm) at a pressure of 5.0×10^{-3} mbar. The DMSO was dosed close to the sample holder to ensure the perfect distribution of the precursor onto the samples. Sample holder temperature was 250ºC. Deposition rate of the silicon oxide films was monitored by a quartz crystal monitor strategically placed close to the deposition area. In these conditions, the SiO_2 deposition rate was 3.5 nm/min.

The microstructure of the films/multilayers was characterized by Scanning Electron Microscopy (SEM) taken in normal and cross section configurations, these latter after dicing the samples deposited onto a silicon wafer. Images were acquired with a field emission microscope (FESEM model Hitachi S4800 at the Instituto de Ciencia de Materiales de Sevilla, CSIC-US, Seville, Spain).

2.2.-Positron annihilation spectroscopy analysis

PA spectroscopy (PAS) is a widely used method for non-destructive characterization of sub- and nanometer-sized open-volume defects in condensed matter by probing the electron density distribution in the material [19]. When positrons (which are antiparticles of electrons) are implanted into condensed matter, they diffuse a specific time until they annihilate with an electron emitting two 511 keV gamma-rays. The energy distribution of the annihilation photons is broadened by the momentum component of the annihilating electron-positron pair. The measurement of this Doppler shift is part of the Doppler Broadening spectroscopy (PAS-DB) and gives information about the electron distribution at the annihilation site. Usually, the spectra are characterized by a shape parameter (S), defined as the fraction of annihilation events with free- and valence electrons, and by a wing parameter (W), defined as the annihilation events with high-momentum core electrons. Whereas the S parameter provides information about the defect concentration, W can be used to identify the elements surrounding the annihilation site.

Atomic empty-volume defects like vacancies or vacancy complexes act as efficient trapping centers for positrons (due to the missing repelling nucleus). Once positrons are trapped there, the annihilation process is delayed due to the lower electron density compared to the defect-free bulk, resulting in a longer positron lifetime. The direct

measurement of the time difference between positron implantation and annihilation is part of the Positron Annihilation Lifetime Spectroscopy (PALS) and can be used to determine the size and distribution of defects.

In insulating solids and at surfaces, positrons can also form a Positronium (Ps) before annihilation which is a hydrogen-atom-like bound state of an electron-positron pair. There are two possible Ps states depending on the relative spin orientation of electron and positron: the singlet state with antiparallel spins is called para-Positronium (p-Ps) and decays into two photons with an intrinsic lifetime of 0.125 ns. The triplet state with parallel spins is known as ortho-Positronium (o-Ps) and decays via 3 photon emission, resulting in a much longer lifetime of 142 ns (in vacuum). When an o-Ps is trapped by pores, the positron involved in o-Ps may annihilate with an electron of the pore wall with opposing spin orientation emitting two photons. The so-called pick - off process significantly reduces the o-Ps lifetime to a few ns in condensed matter. A large pore reduces the probability of this process and increases the o-Ps lifetime. Thus, the measurement of the o-Ps lifetime in the free volume of a material allows the quantitative determination of the pore size [33]. The dependence between the pore size and the positron lifetime is described by a simple shape-free model based on the modified extended Tao-Eldrup model [34]. The pore size can vary from sub-nm to several tens of nm, where the upper limit is given by the intrinsic lifetime of o-Ps in vacuum. For this reason, positron annihilation is only sensitive to small pores within the nanocolumns of the OAD thin films and does not provide information about the large mesopores existing among nanocolumns of these samples.

Since the positron mean implantation depth depends on the particle energy [35], mono-energetic positrons can be used to perform depth-resolved studies of thin films. We performed depth-dependent PALS measurements at the LINAC-based high intense Mono-energetic Positron Source (MePS) [36] whereas DB-PAS measurements were carried out at the isotope-based positron source AIDA/SPONSOR [37, 38], both at the HZDR.

Pore size distributions were calculated from the simple shape-free model of Wada et al. [34] where pore sizes correspond to the long o-Ps related life time components (LTCs). The pore sizes have been estimated for E=4(6) keV in case of multilayers (single SiO_2 and TiO_2 films), which represents roughly the middle region of the films.

2.3.-Simulation of film growth, surface trapping mechanism and calculation of porosity

The growth of the nanocolumnar structures of the films was simulated using a well-accepted simulation code based on Monte Carlo techniques [29], previously published

and released as a simulation package [39]. Making use of this code, we obtained a three-dimensional map of each film formed by effective blocks that correspond to TiO_2 or SiO_2 elements in the material. Values of the trapping probability were taken from the literature, $s_t(TiO_2) = 0.12$ and $s_t(SiO_2) = 1$, while the angular broadening of the angular distribution was set to 6º which, according to ref [18], is adequate for our deposition reactor. The angular incidence for simulation was set to 70º and 85º for both materials and the length of each block was estimated by calculating the typical size of a TiO_2 or SiO_2 block from the density of each material, finding a value of $\sim 0.4\ nm$.

The analysis of the pore size distribution was carry out in two consecutive steps. In a first stage the large intercolumnar void space (i.e., mesopores) was differentiated from other pores (i.e., occluded micropores). For this, we projected a given number of slices of material, n_s, onto one single slice and considered that any empty position in this projected slice corresponds to a pore with length longer than n_s. In this way, any pore with length larger than n_s in the direction of projection can be identified and removed from the analysis. This includes the large mesopores and those embedded pores with length above n_s. Consequently, only pores with size below n_s are considered when calculating the pore size distribution, which in our calculation was taken $n_s = 25\ blocks$, or likewise $\sim 10\ nm$. The calculation of the pore size distribution was carried out in a second step: it was obtained by considering straight lines ranging from each position at the top of the film to its bottom, and calculating the distribution of lengths that corresponds to empty positions.

3.-Results

3.1.-Microstructure of thin films and multilayers

The PAS analysis of pore size distribution in oxide thin films prepared by OAD has been carried out for samples SiO_2-70, SiO_2-85, TiO_2-70 and TiO_2-85 thin films (with and without *capping layer*) and for the SiO_2/TiO_2 multilayer prepared at 70º deposition angle. Films and multilayers consisted of tilted nanocolumns with a diameter of ~100 nm at the surface separated by a large mesopore that extend from the top to the basis of the film [3,4]). The typical nanostructure of these OAD thin films is reported in **Figure 1** showing the cross section micrographs of SiO_2-85 and TiO_2-85 samples. Equivalent images for the SiO_2/TiO_2-85 multilayers are also included in this figure showing that, in this case, nanocolumns of the stacked single TiO_2 and SiO_2 layers arrange in a zig-zag configuration. Additional microstructural analysis of this kind of thin films can be found in previous publications [18, 19, 30, 31].

Visual inspection of the images of the films in Figure 1 reveals a tilted nanocolumnar microstructure for SiO_2-85 and TiO_2-85, where the major difference between both is the tilt angle of the nanocolumns which is higher for TiO_2 (~45º) than for SiO_2 (~25-30º). This behavior is well known in the literature [1-4, 11, 18, 28, 30, 31] and has been attributed to a higher value of the trapping factor for SiO_2 (s_t=1.0) than that for TiO_2 (s_t=0.1).

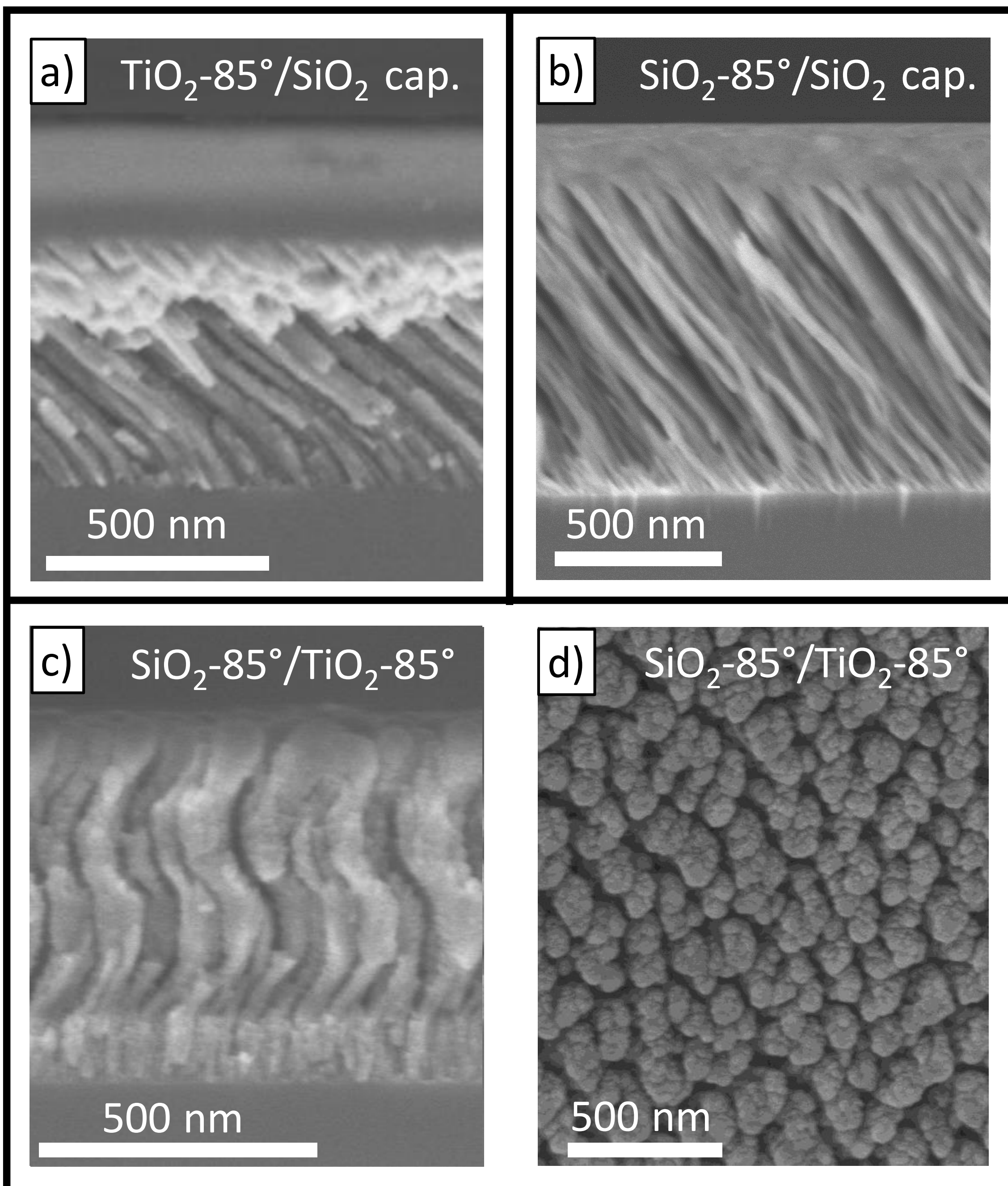

***Figure 1**.- Top) SEM cross section micrographs of SiO_2-85, TiO_2-85 covered with a SiO_2 capping layer. Bottom) Cross section and normal SEM micrographs of a SiO_2-TiO_2 multilayer prepared at 85º deposition angle.*

3.2.-DB-PAS analysis of OAD thin films

Pore analysis in the OAD thin films has been carried out by Doppler broadening positron annihilation spectroscopy (DB-PAS) and PALS. The DB-PAS analysis of the investigated samples revealed a variation of the positron annihilation fraction in different sample zones: capping layer, nanocolumnar film and substrate. The annihilation line parameters

(S and W) are plotted in **Figure 2** as a function of positron implantation energy, Ep, and the mean positron implantation depth, $z_{mean,}$ in SiO_2, represented as top X-axis in the plots. Considering the positron implantation profiles, the maximum positron penetration depth is roughly about $3 \cdot z_{mean}$ [19]. The S-parameter is proportional to defect concentration and/or size, whereas W gives information about defect atomic surrounding, which is not of interest for the current investigation. The similar values of the S and W plots in the capping layer region supports the compact nature of this layer and that its thickness is similar for all the investigated systems. Larger differences are apparent between different investigated films in the film region: (i) SiO_2 films present the highest S values and therefore the highest porosity as compared with the other films, (ii) TiO_2 films have a lower porosity as deduced from their much lower values of S parameters, whereas (iii) multilayers present a dispersion of S parameter values slightly higher but close to those of TiO_2 for Ep>8 keV. The substantial difference in the dispersion of S parameters between SiO_2 and TiO_2 thin films was confirmed by DB-PAS analysis of these thin films without capping layers (see supplementary material, **Figure S1**). A remarkable result from the plots in Figure 2 and Figure S1 is that for each investigated material the curves shape is similar independently on deposition angle. Meanwhile, since the mean positron implantation depth parameter, z_{mean}, is material and porosity dependent (e.g., it is inversely proportional to material density [19]), the plots in Figure 2 and Figure S1 may provide another way of assessing films compactness looking to the variation of the S parameter with z_{mean}. In general, this assessment reveals a similar behavior for the two SiO_2 thin films independently on deposition angle and that only in the case of TiO_2 films at 85º and multilayers there is a certain increase in the S parameter value for Ep>8 keV. This suggests a slightly higher porosity in this case. This suggests a slightly higher porosity in these cases. However, this assessment does not discard the main evidence in the sense that composition and not deposition angle is the main factor controlling the microporosity of OAD thin films. Moreover, all the films exhibit slightly larger S in the film/substrate interface region for the highest deposition angle of α=85°, a feature that we relate with the film compactness. In particular, films deposited at the highest angle have more inclined nanocolumns, larger mesopores and, ultimately, a lower mass thickness, making that positrons reach the substrate at lower E_p.

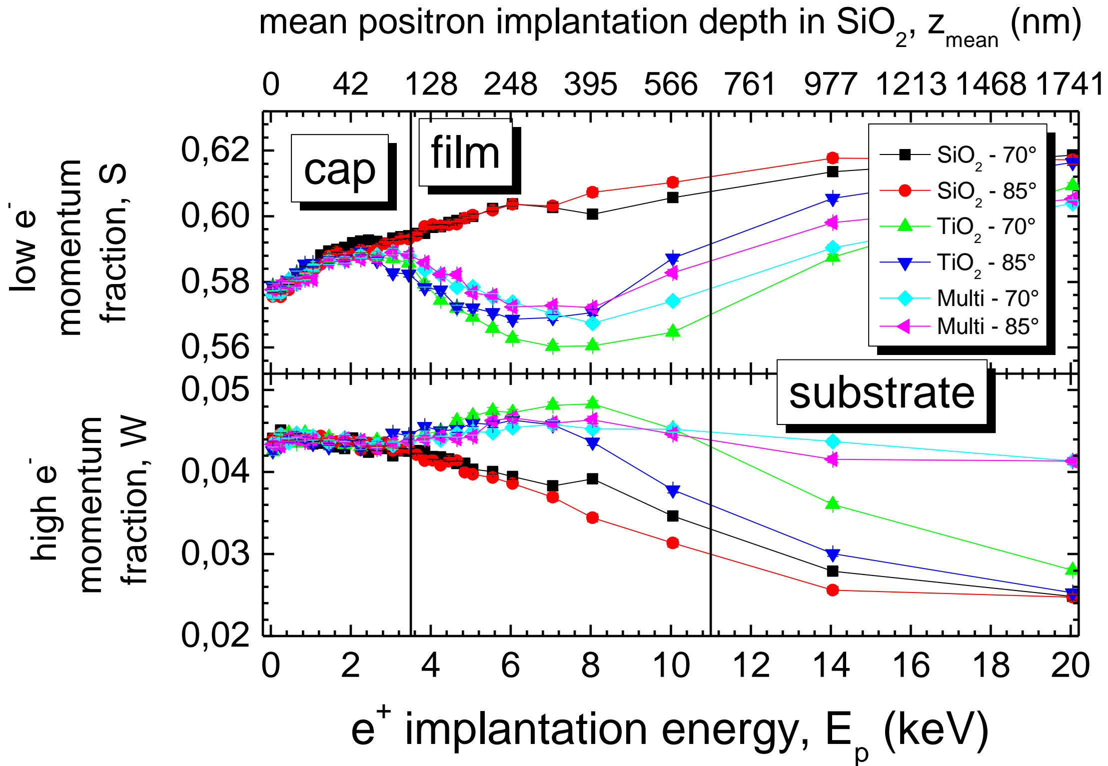

***Figure 2**.- Variation of annihilation line parameters (S and W) as a function of positron implantation energy (E_p). The top X-axis represents a material density dependent mean positron implantation depth for SiO_2 (z_{mean}).*

An additional phenomenon taken place during DB-PAS analysis is the emission of ortho-Positronium (o-Ps). The amount of o-Ps can be estimated as the ratio between 3 gamma annihilation (corresponding o-Ps annihilation in vacuum) to 2 gamma annihilation (corresponding to all other types of annihilation, e.g., localized, free delocalized, pick-off, etc.) [34]. The 3g/2g ratio extracted from DB-PAS spectra for each positron implantation energy, E_p is presented in supplementary materials as **Figures S2 a) and b)** for caped and uncapped systems, respectively. In general, only a small fraction of positrons implanted directly into the sub-surface region of a material (usually with E_p<2keV) can escape as o-Ps. However, for insulating materials of low metallicity like SiO_2, a substantial o-Ps emission can take place even for higher positron energies because of the effect of a favorable image potential formed at the surface [40]. In case of semiconductors and metals, the image potential well is able to trap a large amount of positrons at the surface or in defect states not allowing o-Ps formation at larger energies. For the investigated OAD thin films we observe exactly these phenomena for TiO_2 films and multilayers. In contrast, SiO_2 films show a pronounce maximum in the 3g2g vs E_p plot at E_p≈7keV for the caped α=70° films and much smaller but visible for the caped

α=85° films (Figure S2a)). The situation is even clearer once the cap layer is absent and does not confine the o-Ps within the nanocolumnar structure (see Figure 2Sb). We suggest that the larger o-Ps emission for SiO_2-70° films reflects a relatively larger surface area in these nanostructured films as compared with SiO_2-85 where its much higher mesoporosity reduces the available surface area and makes the o-ps emission less efficient. A maximum surface area has been precisely determined for OAD thin films prepared at 70º zenithal angle of deposition [12].

3.3.-PALS analysis of OAD thin films

PALS analysis utilizing the PALSFIT code [41] of positron annihilation data provides information about the average size of pores (i.e. micropores) and the relative amount of positrons which, reflected by the relative positron life time intensities, annihilate-in a particular type of pore. The summary of data reported in Table 1 (error bar estimation is provided as supplementary material Table S1) reveals at first sight that (i) there are three characteristic pore sizes for SiO_2, (ii) two for multilayers, and (iii) one in the case of TiO_2 nanocolumnar films, and that this distribution of sizes is little affected by the deposition angle. An additional pore size component has been also detected in all samples, d_{int}, corresponding to a positron lifetime value very similar to that found in amorphous SiO_2 [42]. This component reflects to positron annihilation in void defects present in the materials matrix and its detection in all the samples suggests that it can be associated with vacancies in the amorphous structure with a size equivalent to that of one M-O unit (M: Si or Ti). Moreover, to a good approximation, d_1 and d_2 pore sizes for SiO_2 in Table 1 could be attributed to the missing of two or four Si-O units, respectively.

It is also noteworthy in Table 1 that, even though the intensities of positron lifetime component (LTC) corresponding to larger pore sizes, (e.g., d_2 and d_3 for multilayers and TiO_2 films) are sometimes below 1%, their contribution is required in order to obtain a good fit to experimental results and minimize the residuals. Furthermore, since very long positron lifetime components (LTC in the order of 100-140ns) are not detected in these experiments we can conclude that local intercolumnar open volume (i.e. due to the mesopores among nanocolumns, see figure 1) must be above $100nm^3$, a volume for which o-Ps decays after 140ns, outside our measurement time window [34]. It is also remarkable that multilayers depict an intermediate situation between SiO_2 and TiO_2, demonstrating a kind of porosity that is not the average of the porosity of single material films, but a completely new distribution with respect to those found in in the constituent layers. This singular behavior agrees with recent results indicating that the growth mode of a thin film onto another porous and rough layer follows a specific nanostructuration

mechanism [43]. Due to the complexity of these nanostructuration mechanisms they will not be specifically addressed in this paper.

Table 1.- Pore sizes (**d**, in nm) and relative intensities (in %) of LTC deduced from PALS analysis of the investigated samples.*

film	Capping layer	$d_{int}(I_{int})$	$d_1(I_1)$	$d_2(I_2)$	$d_3(I_3)$
		[nm] / [%]			
SiO_2-70	SiO_2	**0.49** (23.72)	**0.89** (1.22)	**1.86** (0.96)	**8.71** (4.32)
SiO_2-85	SiO_2	**0.50** (25.39)	**0.96** (1.51)	**2.12** (0.96)	**8.46** (2.84)
SiO_2-70	no	**0.60** (10.49)	**0.98** (3.12)	**2.09** (4.40)	**8.10** (7.22)
SiO_2-85	no	**0.56** (8.80)	**0.84** (4.45)	**1.99** (4.82)	**8.74** (7.23)
Multi-70	SiO_2	**0.49** (25.43)		**1.56** (0.13)	**4.89** (0.42)
Multi-85	SiO_2	**0.49** (26.88)		**1.54** (0.19)	**6.44** (0.58)
TiO_2-70	SiO_2	**0.49** (23.25)		**2.50** (0.54)	
TiO_2-85	SiO_2	**0.51** (21.99)		**4.37** (0.65)	
TiO_2-70&85	no	**0.40** (2.67)		**3.4** (053)	

- Data are calculated from a simple shape-free model by Wada et al. [34] pore sizes corresponding to the long o-Ps related LTCs (τ_3- τ_6). The pore sizes have been estimated for E=4(6) keV in case of multilayers (single SiO_2 and TiO_2 films), which represents roughly the middle region of the films.

A more detailed insight of the data in this table also reveals that the smallest micropore sizes determined by this analysis were rather similar (within the error of the fit) for the samples with or without capping layer, supporting that positron analysis in this system can be carried out for the OAD samples without preconditioning (however, we must note that absolute pore size values in samples with capping layers might be slightly altered due to the overlapping with the positron annihilation distribution of the cap). Data in Table 1 also show that the size of the largest pores in SiO_2 and TiO_2 films and in the multilayers changes very little with the deposition angle, α, and that the determined values are slightly affected by the presence of a capping layer, very likely because of the already mentioned overlapping effect of film and cap components. Summarizing, although the absolute defect concentration is not accessible with PALS in case of the investigated OAD films, the relative pore sizes (pore populations) can be reliably

estimated. Their relation with the nanocolumn growth mechanism will be discussed in section 3.4 by simulation analysis.

In order to confirm our estimation of pore-size distribution in SiO_2 samples, we carried out an analysis using the advanced MELT code [44]. **Figure 3** shows an exemplary result for SiO_2-70 and SiO_2-85 films. The obtained pore size values correspond well with the results obtained using a discrete data analysis (c.f. Table 1). In addition, the relative intensities obtained by this analysis show that the microporosity in these samples mainly consist of pores with size around 0.5 nm and 8 nm, with a minor contribution of pores with sizes around 0.9 and 1.8 nm.. Similar pore diameters and relative intensities were found for samples deposited on either quartz or silicon substrates, thus supporting that results are not affected by the type of substrate used to grow the films. It is also noteworthy that no evidences about pore size distributions was found by this MELT analysis either for the TiO_2 or the multilayer films. As explained above, we attribute this lack of information to the low intensity of the LTC signal for TiO_2 (c.f., Table 1) which, stemming from the low conversion probability of positrons into o-Ps at the surface, precludes extracting the associated absolute concentration of pores from a PALS analysis.

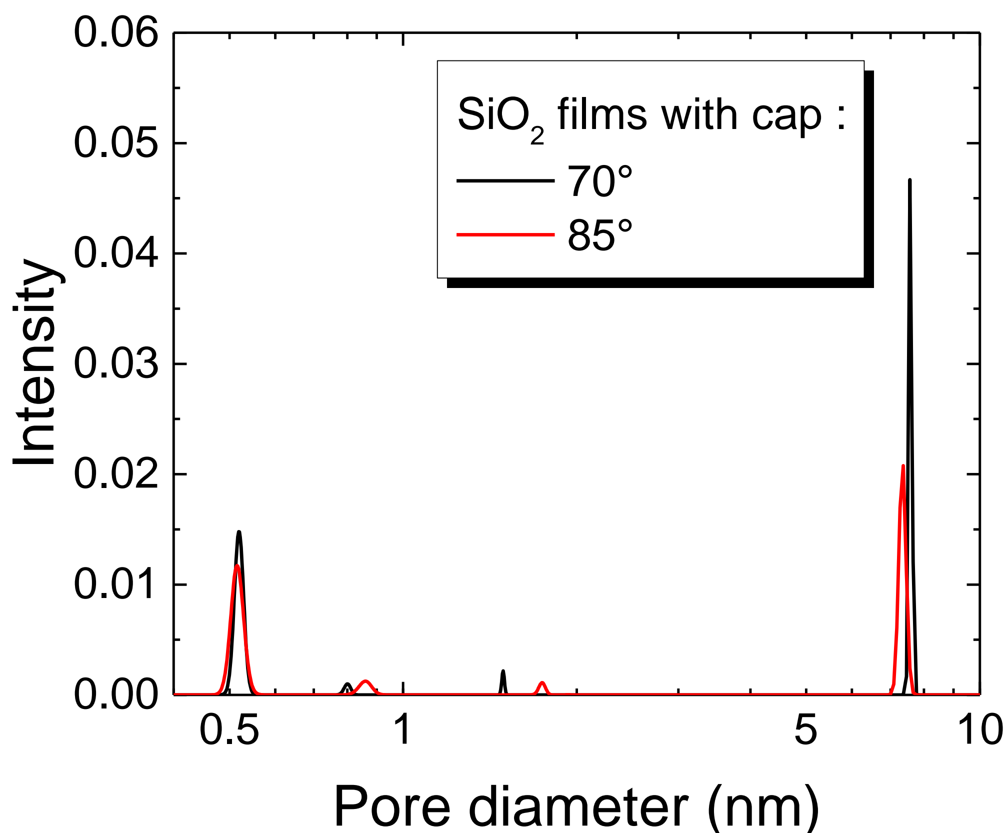

***Figure 3**.- Exemplary analysis utilizing the MELT code [44] to calculate pore size distribution in SiO_2 films.*

3.4.-Thin film growth mechanism and porosity

From the previous analysis by PAS the following main conclusions have been derived: i) for a given material (i.e. TiO_2 or SiO_2) the deposition angle does not significantly affect the porosity inside the nanocolumns, at least for the cases analyzed in the present work; ii) SiO_2 thin films present a higher porosity than TiO_2 thin films, the SiO_2/TiO_2 multilayers representing an intermediate case between the two, and iii) the higher porosity in SiO_2 thin films entails the appearance of micropore sizes larger than in TiO_2. In this way, and since the depositions conditions are the same for each material, the different reported porosity must be somehow linked to fundamental differences in the growth mechanisms and the different chemical composition of the films, which agrees with the very nature of the surface trapping mechanism [18].

Using the methodology described in the experimental section we have simulated the growth of SiO_2 and TiO_2 films for 70º and 85º deposition angles. Cross-sectional views of the simulated films under these conditions have already been published in ref. [18]. Yet, we need to consider that our PAS analysis only provides information on small pores (i.e. micropores), whereas the large pore is excluded, a feature that needs to be taken into account when comparing with simulations. This is of relevance as simulations present the porous structure of the films as a highly connected 3D network, where the large mesopore separating the columns may be weakly or strongly connected to other smaller pores that penetrate into the columns. Hence, a clear criterion must be established on which cavities are considered as part of the mesopore or as an internal pore. In order to differentiate them, we have carried out the projection procedure presented in the Experimental and Methods section by adding different consecutive monolayers of material and checking whether each position is empty (mesopore) or not (internal pore). This procedure ensures that any large pore between columns is identified and removed from the analysis. In **Figure 4** we show the top view of the simulated films after removing the first monolayers from the top and after performing the projection procedure (internal pores are in black). These images clearly show the important differences in terms of porosity among films: TiO_2-70º and TiO_2-85º cases depict a rather different distribution of material due to the different columnar and mesopore features. Yet, pores are similarly distributed with typical lengths of few blocks (below 2 nm), and some larger pores with typical length under 5 nm (see insets in each figure). Remarkably, the cases SiO_2-70º and SiO_2-85º show that columns arrange differently, forming columnar fronts perpendicular to the direction of arrival of deposition species, and likely

associated according to the different trapping efficiency of vapor species. This lateral growth is caused by the so-called lateral trapping mechanism already discussed in ref. [19, 31]. However, in terms of pore size distribution (see insets), pores seems to be rather small with typical lengths between 1 block ($0.4\ nm$) to few blocks. Moreover some large and elongated pores are also evident with typical sizes about $5\ nm$.

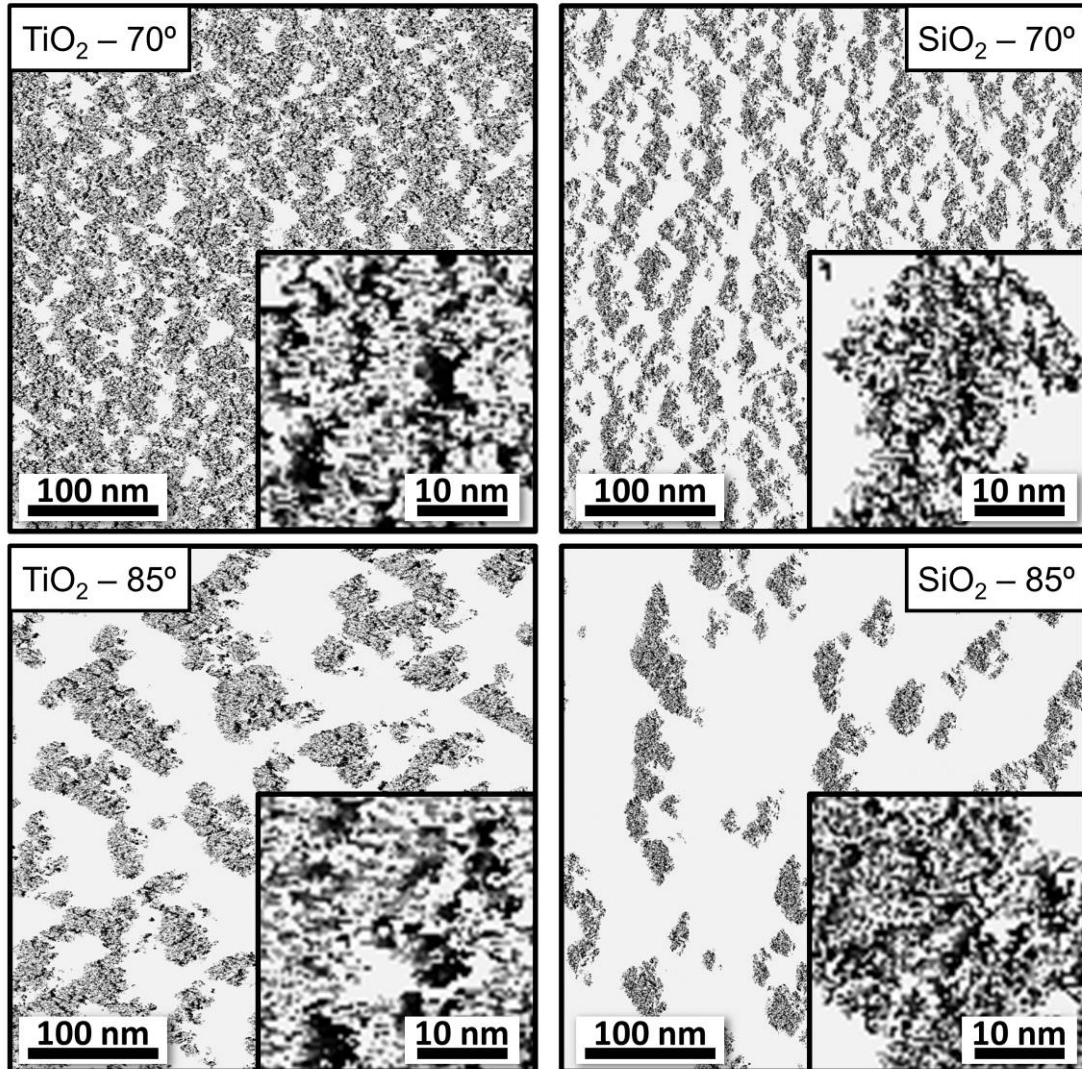

***Figure 4**.- Normal views at different scales of simulated thin films of SiO_2 and TiO_2 prepared at 70º and 85º. They are represented after performing the proposed projection procedure to remove the large mesopore and other pores with size larger than 10 nm (deposition flux arriving from left to right). Pores are shown in black.*

In addition to this visual representation of microporosity in the nanocolumns provided by these images, an assessment of micropore size distributions was done for TiO_2 and SiO_2 thin films using the procedure described in the Experimental and Methods section. The representation of porosity in **Figure 5** in the form of continuous curves show that pore size distribution within the nanocolumns of a given material, SiO_2 or TiO_2, is little affected by the deposition angle (at least for pores with sizes below 10 nm), in agreement with our PAS analysis. It also reveals the distribution of both small and big size pores for SiO_2

and TiO_2 thin films, indicating that TiO_2 contains a larger proportion of pores with sizes below 1.2 nm, while SiO_2 contains a larger proportion of larger pores, in agreement with the data in Table 1. Moreover, the rather flat distribution of pores with sizes below 2 nm for SiO_2 indicates the existence of a large proportion of pores with different sizes for SiO_2 in comparison with TiO_2, where the distribution curve falls rapidly. It is noteworthy that the area below the curves (note the logarithmic scale) is greater for SiO_2 than for TiO_2 thin films, indicating a higher volume of pores in the former in good agreement with the DB-PAS results in Figure 2.

The evidences deduced from the simulation analysis agree with the experimental PA results regarding the main feature of the internal pore size distribution, namely a similar micropore distribution for each material independently on deposition angle, the higher microporosity volume in SiO_2 than in TiO_2 OAD thin films and the existence of some larger pores in SiO_2 thin films. In relation with the parameters controlling the growing mechanism of the films, our analysis confirms the correlation of the higher volume of micropores in the nanocolumns of SiO_2 thin films with the higher trapping coefficient of this material during its OAD growth.

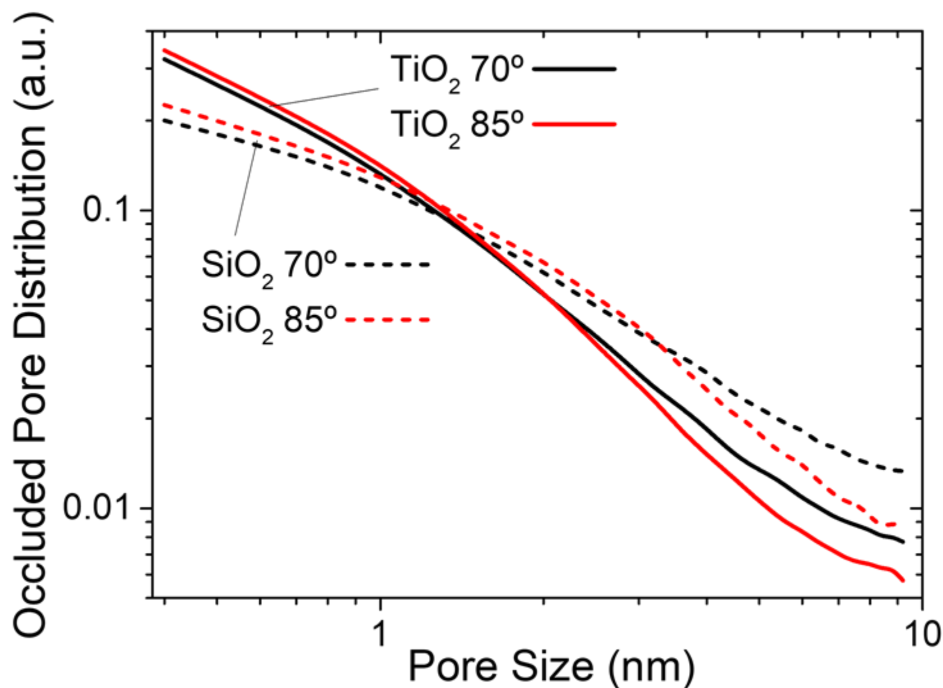

Figure 5.- *Calculated pore size distribution normalized to the total amount of embedded void space of micropores in each case.*

4.-Conclusions

In this work we have studied by PAS analysis the microporosity existing in the nanocolumns forming the basic microstructural elements of oblique angle deposited thin films. The comparative analysis of TiO_2 and SiO_2 thin films has shown a higher concentration and size of micropores in the latter case, while no significant differences were found as a function of the deposition angles, at least for the relatively large zenithal angles (i.e. 70º and 85º) utilized for the preparation of the studied samples. The Monte Carlo simulation analysis of the porosity of these thin films under the assumption of a trapping mechanism of the deposition particles renders a similar distribution of micropores. The agreement between experiment and simulation proves that the trapping mechanism is responsible for the development of the particular microstructure and internal microporosity of oblique angle deposited thin films. These results confirm the validity of the utilized methodology and open the way for a systematic analysis of thin film microstructure using PA to describe the growth processes of thin films.

5.-Acknowledgements

The authors thank the European Regional Development Funds program (EU-FEDER) and the MINECO-AEI (MAT2016-79866-R) and CSIC (201560E055, 201860E050) for financial support. We also acknowledge the support of the University of Seville (V and VI PPIT-US. Positron annihilation experiments were carried out in the ELBE facility thanks to the large infrastructure program of the EU (proposal no. POS16200743). We acknowledge BMBF for the PosiAnalyse (05K2013) grant, the Impulse- und Networking fund of the Helmholtz-Association (FKZ VH-VI-442 Memriox), and the Helmholtz Energy Materials Characterization Platform (03ET7015).

References

[1] A. Barranco, A. Borras, A. R. Gonzalez-Elipe, A. Palmero. Perspectives on oblique angle deposition of thin films: From fundamentals to devices. Progr. Mater. Sci. 76 (2016) 59–153.

[2] M.M. Hawkeye, M.T. Taschuk, M.J. Brett. Glancing angle deposition of thin films: engineering the nanoscale. Wiley Series in Materials for Electronic & Optoelectronic Applications; 2014.

[3] K.M. Krause, M. Thommes, M.J. Brett. Pore analysis of obliquely deposited nanostructures by krypton gas adsorption at 87 K. Micropor. Mesopor. Mat. 143 (2011) 166-173.

[4] L. Gonzalez-Garcia, J. Parra-Barranco, J.R. Sanchez-Valencia, A. Barranco, A. Borras, A.R. Gonzalez-Elipe, M.C García-Gutierrez, J.J. Hernández, D.R. Rueda, T. Ezquerra. Correlation lengths, porosity and water adsorption in TiO2 thin films prepared by glancing angle deposition. Nanotechnology 23 (2012) 205701-205711.

[5] H. Z. Yu, C. V. Thompson. Effects of oblique-angle deposition on intrinsic stress evolution during polycrystalline film growth. Acta Mater. 77 (2014) 284–293.

[6] M.F. Parkinson, J.K. Ko, A. Halajko, S. Sanghvi, G.G. Amatucci. Effect of vertically structured porosity on electrochemical performance of FeF_2 films for Lithium batteries. Electrochim. Acta 125 (2014) 71-82.

[7] Y. Zhou, T. Taima, T. Miyadera, T. Yamanari, M. Kitamura, K. Nakatsu, Y. Yoshida. Glancing angle deposition of copper iodide nanocrystals for efficient organic photovoltaic. Nano Lett. 12 (2012) 4146-4152.

[8] Y. Liu, A. Rzhevskii, S. Rigos, W.Y. Xie, S.B. Zhang, T.M. Lu, G.C. Wang. A study of parylene coated Pd/Mg nanblades for reversible hydrogen storage. Int. J. Hydrogen Energy 38 (2013) 5019-5029.

[9] H. G. Moon, Y.R. Choi, Y.S. Shim, I.K. Choi, J.H. Lee, J.S. Kim, S.J. Yoon, H.H. Park, C.Y. Kang, H.W. jang. Extremely sensitive and selective no probe based on villi-like WO3 nanostructures for application to exhaled breath analyzers. ACS Appl. Mater. Interfaces 5 (2013) 10591-10596.

[10] M.M. Hawkeye, M.J. Brett. Optimized colorimetric photonic crystal humidity sensor fabricated using glancing angle deposition. Adv. Funct. Mater. 21 (2011)3652-3658.

[11] D.W. Flaherty, N.T. Hahn, R.A. May, S.P. Berglund, Y.M. Lin, K.J. Stenvenson, Z. Dohnalek, B.D. Kay, C.B. Mullins. Reactive ballistic deposition of nanostructured model materials for electrochemical energy conversion and storage. Acc. Chem. Res. 45 (2012) 434-443.

[12] M. Suzuki, Y. Taga. Numerical study of the effective surface area of obliquely deposited thin films. J. Appl. Phys. 90 (2001) 5599-5607.

[13] S.J. Gregg, K.S.W. Sing. Adsorption, surface area and porosity. London. Academic Press 1982.

[14] S. Liedtke, C. Grüner, A. Lotnyk, B. Rauschenbach. Glancing angle deposition of sculptured thin film metal films at room temperature. Nanotechnology 28 (2017) 385604.

[15] T. Karabacak, G.C. Wang, T.M. Lu. Quasi-periodic nanostructures grown by oblique angle deposition. J. Appl. Phys. 94 (2003) 7723-7728.

[16] J. M. Nieuwenh, H.B. Haanstra. Microfractography of thin films. Philips Tech. Rev. 27 (1966) 87-91.

[17] R.N. Tait, T. Smy, M.J. Brett. Modelling and characterization of columnar growth in evaporated films. Thin Sol. Films 226 (1993) 196-201.

[18] R. Alvarez, C. Lopez-Santos, J. Parra-Barranco, V. Rico, A. Barranco, J. Cotrino, A. R. Gonzalez-Elipe, A. Palmero. Nanocolumnar growth of Thin films deposited at oblique angles: Beyond the tangent rule. J. Vac. Sci. Technol. B 32 (2014) 041802 1-6.

[19] R. Krause-Rehberg and H. S. Leipner, Positron annihilation in semiconductors: defect studies, Springer, 1999.

[20]] YC, J. J., & Schrader, D. M. (Eds.). (2003). Principles and applications of positron and positronium chemistry. World Scientific.

[21] D.W. Gidley, H.G. Peng, R.S. Vallery. Positron annihilation as a method to characterize porous materials. Annu. Rev. Mater. Res., 36 (2006) 49-79.

[22] A. Cabral-Prieto, I. García-Sosa, R. López-Castañares, O. Olea-Cardoso. Positronium annihilation in LTA-type zeolite. Micropor. Mesopor. Mat., 175 (2013) 134-140.

[23] K.M. Flores. E. Sherer. A. Bharathula. H. Chen. Y.C. Jean. Sub-nanometer open volume regions in a bulk metallic glass investigated by positron annihilation. Acta Mater. 55 (2007) 3403-3411.

[24] M. Elsayed. R. Krause-Rehberg. As-vacancy complex in Zn-diffused GaAs: Positron lifetime spectroscopy study. Scripta Mater. 131 (2017) 72-75.

[25] C.-H. Lo, K.-S. Liao, W.-S. Hung, M. De Guzman, C.-C. Hu, K.-R. Lee, J.-Y. Lai. Investigation on positron annihilation characteristics of CO2-exposed zeolite. Micropor. Mesopor. Mat. 141 (2011) 140-145.

[26] M.A. Noah. D. Flototto. Z.M. Wang. M. Reiner. M. C. Hugenschmidt. E.J. Mittemeijer. Interdiffusion in epitaxial, single-crystalline Au/Ag thin films studied by Auger electron spectroscopy sputter-depth profiling and positron annihilation. Acta Mater. 107 (2016) 133-143.

[27] P. Parente. Y. Ortega. B. Savoini. M.A. Monge. A. Tucci. L. Esposito. A-J. Sanchez-Herencia. Microstructural characterization of alumina-zirconia layered ceramics using positron annihilation spectroscopy. Acta Mater. 58 (2010) 3014-3021.

[28] R Alvarez, L. Gonzalez-Garcıa, P Romero-Gomez, V Rico, J Cotrino, A R Gonzalez-Elipe, A Palmero. Theoretical and experimental characterization of TiO2 thin films deposited at oblique angles. J. Phys. D: Appl. Phys. 44 (2011) 385302.

[29] R Alvarez, J M García-Martín, M Macías-Montero, L Gonzalez-Garcia, J C González, V Rico, J Perlich, J Cotrino, A R González-Elipe, A Palmero. Growth regimes of porous gold thin films deposited by magnetron sputtering at oblique incidence: from compact to columnar microstructures. Nanotechnology 24 (2013) 045604 1-9.

[30] L. González-García, J. Parra-Barranco, J.R. Sánchez-Valencia, J. Ferrer, M.C. García-Gutierrez, A. Barranco, A.R. González-Elipe Tuning Dichroic Plasmon Resonance Modes of Gold nanoparticles in Optical Thin Films. Adv. Funct. Mater. 23 (2013) 1655-1663.

[31] C. López-Santos, R. Alvarez, A. García-Valenzuela, V. Rico, M. Loeffler, A.R. González-Elipe, A. Palmero. Nanocolumnar association and domain formation in porous Thin films grown by evaporation at oblique angles. Nanotechnology 27 (2016) 395702 1-9.

[32] M. Oliva-Ramirez, A. Barranco, M. Löffler, F. Yubero,A. R. González-Elipe. Optofluidic Modulation of Self-Associated Nanostructural Units Forming Planar Bragg Microcavities. ACS Nano 10 (2016) 1256−1264.

[33] M. Gorgol, M. Tydda, A. Kierys, R. Zaleski. Composition of pore surface investigated by positron annihilation lifetime spectroscopy. Micropor. Mesopor. Mat. 163 (2012) 276-281.

[34] K. Wada, T. Hyodo. A simple shape-free model for pore-size estimation with positron annihilation lifetime spectroscopy. J. of Phys.: Confer. Series 443 (2013) 012003 1-4.

[35] V. J. Ghosh, B. Nielsen, K. G. Lynn, D. O. Welch. Defect profiling in elemental and multilayer systems: correlations of fitted defect concentrations with positron implantation profiles. Appl. Surf. Sci. 85 (1995) 210-215.

[36] A. Wagner, M. Butterling, M. O. Liedke, K. Potzger, R. Krause-Rehberg. Positron annihilation lifetime and Doppler broadening spectroscopy at the ELBE facility. AIP Confer. Proceed. 1970 (2018), 040003 1-8.

[37] W. Anwand, G. Brauer, M. Butterling, H. R. Kissener, A. Wagner. Design and Construction of a Slow Positron Beam for Solid and Surface Investigations. Defect Diffus. Forum 331 (2012) 25-40.

[38] M.O. Liedke, W. Anwand, R. Bali, S. Cornelius, M. Butterling, T.T. Trinh, A. Wagner, S. Salamon, D. Walecki, A. Smekhova, H. Wende, K. Potzger, Open volume defects and magnetic phase transition in Fe 60 Al 40 transition metal aluminide, J. Appl. Phys. 117 (2015) 163908.

[39] Nanotechnology on Surfaces: Computer Programs and Simulations https://nanoscops.icmse.csic.es/software/ (accessed 16 September 2019)

[40] R. Nieminen, M. Manninen. Positron surface states in metals. Sol. State Commun. 15 (1974) 403-406.

[41] J.V. Olsen, P. Kirkegaard, N.J. Pedersen, M. Eldrup, PALSfit: A new program for the evaluation of positron lifetime spectra. Phys. Status Solidi C 4 (2007) 4004-4006.

[42] S. Dannefaer, T. Bretagnon, D. Kerr. Vacancy-type defects in crystalline and amorphous SiO2. J. Appl. Phys. 74 (1993) 884-890.

[43] A Garcia-Valenzuela, C Lopez-Santos, R Alvarez, V Rico, J Cotrino, A R Gonzalez-Elipe, A Palmero. Structural control in porous/compact multilayer systems grown by magnetron sputtering Nanotechnol. 28 (2017) 465605 1-9.

[44] A. Shukla, L. Hoffmann, A.A. Manuel, M. Peter. Melt 4.0 a Program for Positron Lifetime Analysis. Mater. Sci. Forum, 255-257 (1997) 233-237.